Available online at www.sciencedirect.com
SCIENCE DIRECT®
C. R. Mecanique 332 (2004) 375–386
COMPTES RENDUS MECANIQUE

Microgravity and Transfers/Interfaces and phase change, two-phase flow

Multiphase computations using sharp and continuous interface techniques for micro-gravity applications

Wei Shyy

Department of Mechanical and Aerospace Engineering, University of Florida, Gainesville, FL 32611, USA

Abstract

The Eulerian–Lagrangian method is a popular and effective approach for handling multi-fluid problems involving substantial shape variations. Specifically, one can consider the interface either as a sharp discontinuity, consistent with the fundamental continuum theory, or as a smooth transition zone, reducing numerical difficulties in tracking distinct regions. In this article, we highlight the performance characteristics of both techniques. Computationally, both approaches can be devised using similar concepts, namely, the interface is represented by marker points and advected in a Lagrangian framework, and the mass, momentum, and energy conservation equations are solved on a fixed (Eulerian) Cartesian grid using a second-order projection method. The main difference lies in the way of accounting for the interfacial conditions and communication across the interface. The sharp interface method is more demanding computationally because the field equations in each zone need to be coupled with those in other materials/phases, by explicitly tracking the interfacial conditions via matching procedures. In return, second-order accuracy can be attained as compared to the first-order accuracy in the continuous interface method. Nevertheless, in physical applications, both approaches can be highly effective in handling a variety of multi-fluid problems involving moving boundaries. Several examples are presented to highlight the various performance characteristics of the two techniques. ***To cite this article: W. Shyy, C. R. Mecanique 332 (2004).***

Résumé

Techniques de calcul numérique pour frontières mobiles. La méthode eulerienne–lagrangienne offre une approche populaire et efficace pour traiter des problèmes multi-fluidiques comportant des variations de forme. Spécialement, quand l'interface est considérée comme une discontinuité, consistante avec la théorie du milieu continu, ou comme une transition continue rapide, réduisant les difficultés numériques pour marquer les différentes régions. Dans ce papier, des éclaircissements sont apportés sur la performance des deux techniques. Sur le plan numérique, les deux approches sont développés sur des concepts similaires, l'interface est représentée par des marqueurs soumis à l'advection dans le sens lagrangien et les équations de conservation de la masse, de la quantité de mouvement et de l'énergies sont résolues sur une grille cartésienne fixe (eulerienne) à l'aide d'une méthode de projection de second ordre. La différence essentielle réside dans la manière de prendre en compte les conditions de transmission à l'interface. La méthode où l'interface est considérée comme une discontinuité demande un effort supplémentaire au sens numérique parce que le champ de vitesses dans chaque zone doit être couplé avec ceux dans les autres matériaux/phases, en assurant explicitement les conditions de transmission à l'interface par des procédures de raccordement. Par contre, une précision de second ordre pent être obtenue en comparaison avec le premier ordre de la méthode de l'interface continue. Néanmoins, pour des applications physiques, les deux approches peuvent être très efficaces pour traiter une variété de

E-mail address: wei-shyy@ufl.edu (W. Shyy).

1631-0721/$ – see front matter
doi:10.1016/j.crme.2004.02.014

problèmes multi-fluides qui comportent des frontières mobiles. Plusieurs exemples sont apportés pour illustrer les performances des deux techniques. ***Pour citer cet article : W. Shyy, C. R. Mecanique 332 (2004).***

Keywords: Computational fluid mechanics; Moving boundary problems; Multiphase systems; Micro-gravity science

Mots-clés : Mécanique des fluides numérique ; Problèmes des frontières mobiles ; Système multiphase

1. Introduction

Multiphase flows, such as those involving droplets and bubbles, are frequently encountered in both micro- and normal-gravity conditions. Under micro-gravity applications, frequently, the interfacial dynamics becomes important and the moving boundary needs to be tracked carefully in order to understand the associated fluid physics. These problems are not easy to simulate accurately due to the fact that they involve interfaces with unknown and time varying shapes. Numerous techniques have been developed for tracking interfaces between separating materials, phases and properties. Categorically, there are moving grid (Lagrangian) [1–4] and fixed grid (Eulerian) approaches [4–6]. The main challenges for moving boundary computations include:

- Mass conservation within individual and overall domain;
- Numerical instabilities and wiggles caused by the property and flux discontinuities at the interface;
- Errors associated with calculating the geometric quantities, especially curvature, of the interface;
- 2D (planar or axisymmetric) models for phase transport may become very complicated in 3D;
- Convergence problems for high density (viscosity) ratio or large surface tension;
- Objects break-up and coalescence;
- Difficulty of achieving more than first order accuracy.

In the fixed grid approach, one can resort to the purely Eulerian approach such as the volume of fluid method [6, 12] for free surface flows, or the enthalpy formulation [7,8] when phase change is involved. In these methods, the interface is constructed after the field solution is obtained. In the purely Eulerian approach, the interface construction is decoupled from the field equation solver, which can cause difficulties such as uniqueness of the shape interpretation, and continuity and smoothness of the interface.

Alternatively, one can also employ the Eulerian–Lagrangian method, which explicitly tracks the interface utilizing the fixed grid with the aid of the Lagrangian component. Alternative approaches have been proposed in this category. In particular, the continuous interface method (CIM), such as the immersed boundary technique [5,8] or the level set method [9], has been popular. CIM defines the interface as a smooth transition zone and can be conveniently coupled with the field equations. With this approach, the interface is of finite thickness, which reduces the order of accuracy of the overall solution to first order [10–12], or even lower. For example, a spurious velocity field can appear in the interface region [11,12]. While improved treatments can reduce the magnitude of the spurious velocity [12], in general, its presence and influence is non-negligible.

In the context of the Eulerian–Lagrangian method, the sharp interface method (SIM) has also been developed [13–17]. In SIM, the interface is considered to be a discontinuity separating two materials, with the field equations handled by the fixed grid, while directly accounting for the presence of the interface by forming irregularly shaped computational cells. At the modeling level, SIM is consistent with the concept of continuum mechanics because the interface is considered to be of zero thickness and there is no smearing in the algorithm to link individual phases/materials. As demonstrated in [16], for fixed geometry problems, and in [15], for one-dimensional moving boundary problems, SIM can maintain second order accuracy. However, for cases involving curved free boundaries, no rigorous investigation of the performance of the sharp interface method has been performed.

In this article, we assess the interfacial characteristics, in regard to the spurious velocity and the pressure distributions, of SIM and CIM approaches for a static drop under the influence of capillarity and hydrostatic pressures. Next, we highlight solutions obtained for drop dynamics to illustrate the effect of capillarity and heat transfer associated with the impact dynamics.

2. Analysis and modeling

The field equations for mass, momentum and energy transport, along with the corresponding interfacial conditions, can be found in [7,10,22]. In the following, we highlight the salient features associated with SIM and CIM.

2.1. Sharp Interface Method (SIM)

The present sharp-interface method employs a combined Eulerian–Lagrangian strategy. As discussed in details in [15–17], the present SIM has the following distinguishing features:

- the finite-volume method is adopted to ensure the conservation of mass, momentum and energy transport in each phase/material;
- specific governing equations are constructed for each phases/materials, instead of using the single set of governing equations for the entire domain of all phases/materials. This enables the method to handle large property (such as density) ratios across the interface with relative ease;
- sharp-interface with no numerical smearing;
- interfacial constraints are imposed as distinct boundary conditions, instead of being incorporated through source terms in the governing equations;
- the C^2 cubic B-spline curve fitting method is employed to represent the interface [16,18]. A fairing algorithm for curvature calculation makes it possible to use the current SIM to compute problems in which accurate curvature estimation is critical for simulating interfacial dynamics.

In addition, the present SIM also has the capability to treat the phase change at the interface. An illustration of the cell and interface intersection treated in the sharp-interface method is depicted in Fig. 1. It is noted that the small fragments of cut-cells are absorbed into the neighboring cells in the same phase to form larger, trapezoid cells. The interface, represented by suitable geometric representations based on massless markers, intersects with the underlying, fixed Cartesian grid. A compact interpolation method near the interface is adopted to retain second-order accuracy and conservation property.

2.2. Continuous Interface Method (CIM) based on the immersed boundary technique

In this approach, the interface discontinuity is treated by the immersed boundary method originally presented by Peskin [5]. The interface is considered to be of small non-zero thickness within which the fluid properties change smoothly. An illustration of a typical computational domain composed of two immiscible fluids is given in Fig. 2(a). The fluid domain denoted by Ω is covered with a fixed Cartesian grid. The interface between Fluid 1 and Fluid 2, represented by the curve C, is present in the fluid domain Ω and is marked by particles (dots) that do not coincide with the grid points. In the immersed boundary method, the information between the moving interface and the field variables is exchanged through interpolation. Since the locations of the marker points in general do not coincide with the underlying grid points employed to solve the field equations, the velocity of the field equation, defined according to the Cartesian grid system is interpolated to obtain the marker velocity. The concept is illustrated in

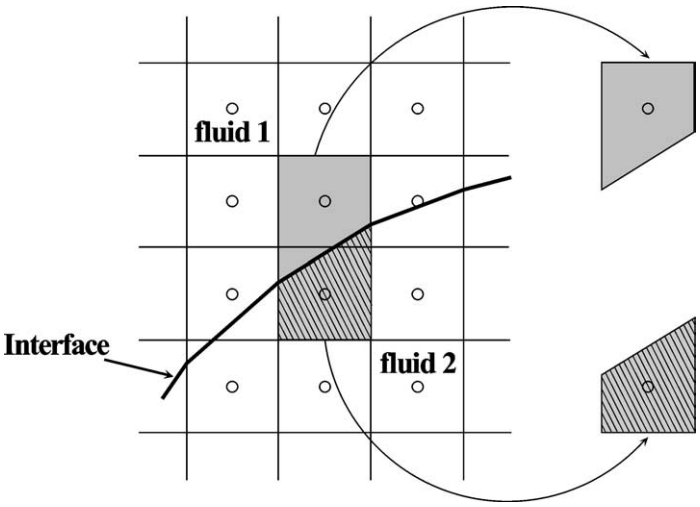

Fig. 1. Illustration of the cell-interface intersection in the sharp interface method. Trapezoidal cells are formed near the interface.

Fig. 1. Illustation de l'intersection cellule-interface pour la méthode de l'interface discontinue. Des cellules trapézoïdales sont formées au voisinage de l'interface.

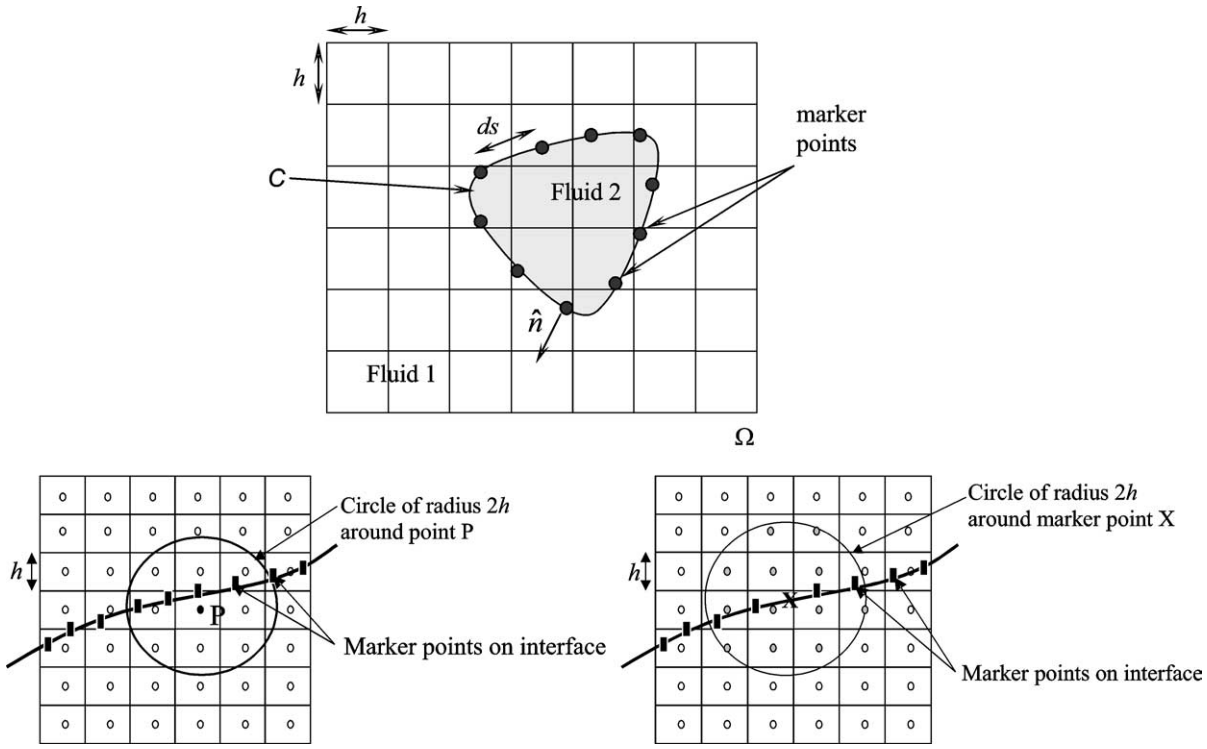

Fig. 2. Main features of the immersed boundary technique: (top) schematic of two immiscible fluids; (left) marker points considered for the estimation of the force at point P; (bottom) grid points considered for the interface velocity around the marker X.

Fig. 2. Caractéristiques principales de la technique des frontières mobiles : (dessus) dessin de deux fluides immiscibles ; (gauche) marqueurs considérés pour l'estimation de la force au point P ; (droite) maillage considéré pour la vitesse interfaciale autour du marqueur X.

Figs. 2 (b) and (c). With the interface location known with respect to the grid, the material properties are assigned in each fluid based on a Heaviside step function. For example the density ρ is distributed as

$$\rho = \rho_1 + (\rho_2 - \rho_1) H(\xi) \tag{1}$$

where $H(\xi)$ is the discrete Heaviside step function defined here as:

$$H(\xi) = \begin{cases} 0 & \text{if } \xi \leqslant -\gamma \\ 1 & \text{if } \xi \geqslant +\gamma \\ \prod_{m=1}^{\dim} \frac{1}{2}\left(1 + \frac{\xi_m}{\gamma} + \frac{1}{\pi}\sin\frac{\pi\xi_m}{\gamma}\right) & \text{otherwise} \end{cases} \tag{2}$$

In the above equation, $\xi = \mathbf{x} - \mathbf{x}_k$, dim is the space dimension, $\gamma = 2h$ is the transition distance where h is the cell width, $\mathbf{x}$ is the grid coordinate, and $\mathbf{x}_k$ is the interfacial marker coordinate. Since the location of the Lagrangian interface points does not coincide with the fixed Eulerian grid points, the velocity field stored at the cell-center of each grid is interpolated to obtain the velocity of the interface points, and the interface force acting on the marker points is spread to the nearby grid points via a discrete Delta function. The discrete Delta function in this study is taken as:

$$\delta(\xi) = \begin{cases} \prod_{m=1}^{\dim} \frac{1}{2\gamma}\left(1 + \cos\frac{\pi\xi_m}{\gamma}\right) & \text{if } |\xi| \leqslant \gamma \\ 0 & \text{otherwise} \end{cases} \tag{3}$$

At each time step, the interface position is advected in a Lagrangian way and a procedure to enforce mass conservation of the droplet within specified criteria (here taken as 0.01%) is applied.

2.3. Solution procedure

The projection method or fractional-step method is employed to solve the coupled mass and momentum equations. Specifically, the second-order accurate, two-step fractional step method presented in Ye et al. [16,17] and Francois and Shyy [22] is used to solve the flow equations. The mass and momentum equations are discretized using a finite-volume formulation on a fixed Cartesian mesh using a cell-centered collocated arrangement for all the variables. As detailed in [17], to ensure mass conservation, a face-cell velocity variable is introduced for computing the volume flux. The convection terms are discretized with a second order accurate Adams–Bashforth scheme, the diffusion terms with a second order Crank–Nicolson scheme. To speed up the computation, a multigrid technique can be employed to solve the pressure equation [22,23].

3. Results and discussion

3.1. Interfacial characteristics of a static drop

For the present test problem, the density ratio ρ_l/ρ_v between the liquid drop and surrounding gas varies from 1 to 1000. The largest ratio corresponds to the circumstance between water and air under the standard atmospheric condition. With a spherical drop in static equilibrium, there are two uniform pressure fields inside and outside of the drop boundary, namely, the pressure inside is $p_0 + 2\sigma/R$ and outside is p_0. The difference balances the surface tension effect, according to the Young–Laplace condition [7]:

$$\Delta p_{\text{exact}} = \frac{2\sigma}{R} \tag{4}$$

where σ is the surface tension and R is the radius of the droplet. In the present study, σ is set to 1.0 N/m and R equals to 0.25 m; the exact pressure difference Δp_{exact}, therefore, should be equal to 8.0 N/m^2. The numerical result of the pressure difference is compared against this exact value.

In the present study, the drop is located at the center of a circular cylinder. Both the height and the diameter of the cylinder are twice the drop diameter. Given the axi-symmetric nature of the problem, only half of the computational domain is considered, with the bottom boundary being the symmetric axis. On other boundaries of the domain, zero viscous stress conditions are specified for velocity field and the zero gradient condition is adopted for pressure. A fixed, uniform Cartesian grid is employed. The initial condition consists of constant pressure in the entire domain, with different density values assigned inside and outside of the drop.

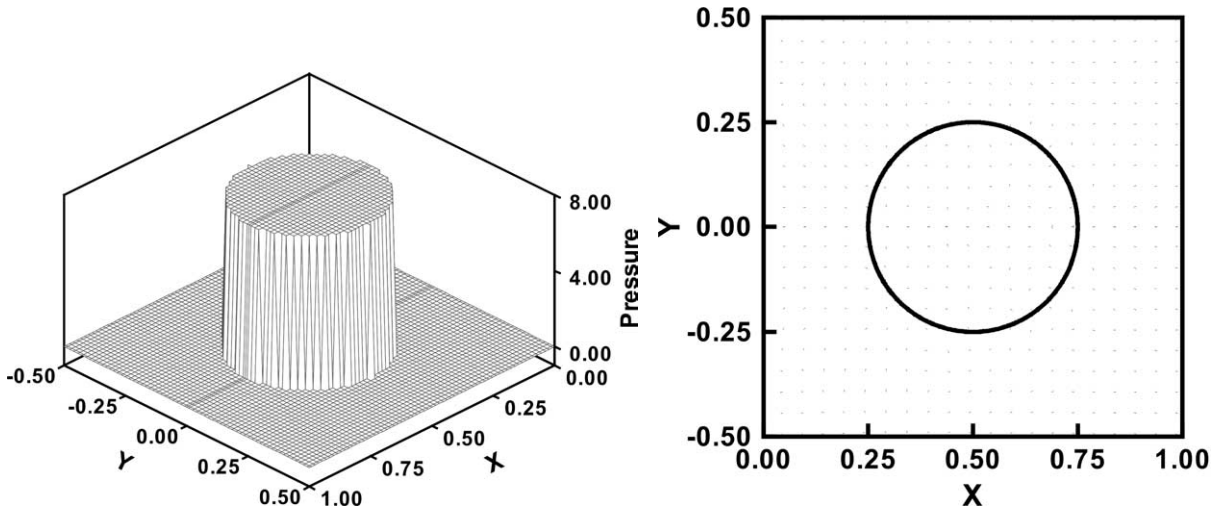

(a) (b)

Fig. 3. The overall pressure and velocity distributions for a drop in static equilibrium (a) pressure, (b) velocity vectors. The maximum values of the u- and v-component of the spurious velocity are 4.687×10^{-10} and 4.279×10^{-10}, respectively.

Fig. 3. Distribution des pressions et des vitesses pour une goutte en équilibre statique (a) pression, (b) vecteurs vitesse. Les valeurs maximales des composantes u et v de la vitesse fluctuante sont $4{,}687 \times 10^{-10}$ et $4{,}279 \times 10^{-10}$, respectivement.

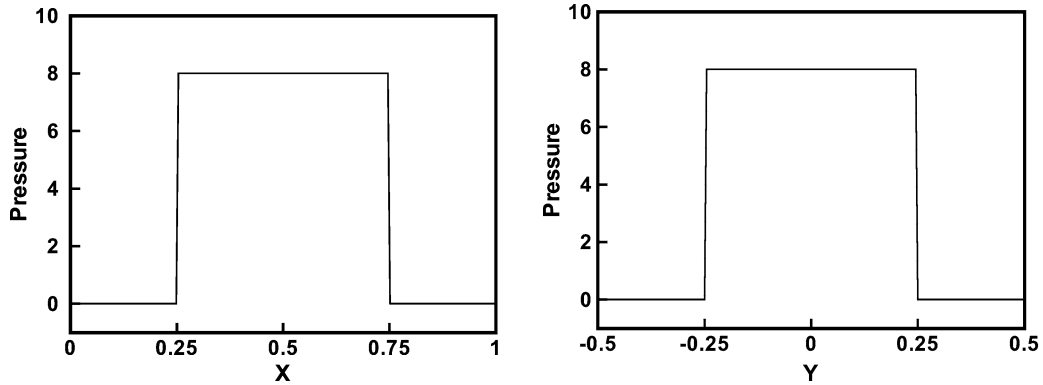

Fig. 4. Pressure profiles along the horizontal and vertical center lines.

Fig. 4. Profils de pression le long des lignes centrales horizontale et verticale.

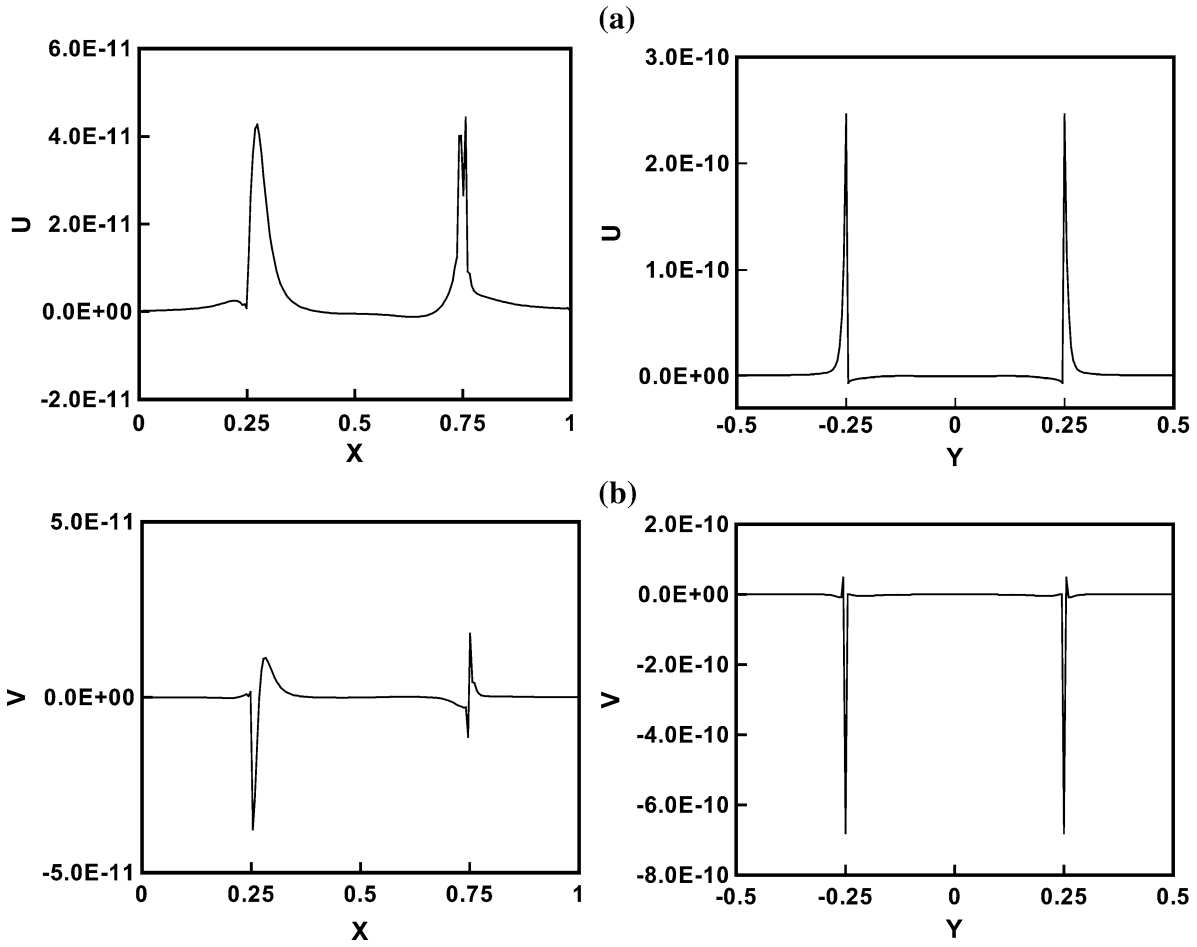

Fig. 5. Velocity profiles along the horizontal and vertical center lines: (a) horizontal-velocity component; (b) vertical-velocity component.

Fig. 5. Profils de vitesse le long des lignes centrales horizontale et verticale : (a) composante horizontale de la vitesse ; (b) composante verticale de la vitesse.

The case with a density ratio of 1000 is considered first. Unless noted otherwise, the ratio of the drop radius to the grid size, $R/\Delta x$, is 50, namely, with 100×200 grid (along radial and longitudinal directions, respectively) covering the entire computational domain. Fig. 3 shows the pressure distribution and velocity vectors (with all vectors set to be of the unit magnitude) in the domain. Detailed profiles along both horizontal and vertical directions are shown in Fig. 4. Figs. 3 and 4 demonstrate that the sharp interface method with the cut-cell treatment can capture the crisp pressure distribution across the interface. Fig. 5 depicts the profiles of the velocity components in both x and y directions. In contrast to CIM (see, e.g., [19]), which typically yields substantial spurious velocity, SIM produces errors virtually at the round-off level. The curvature computation is a key in many interfacial transport problems; they are also very difficult to compute accurately because of the non-linear combination of first and second derivatives. To assess the performance of SIM, Fig. 6 presents the computed curvature, plotted along the entire circumference of the drop boundary. An accurate estimation has been obtained with little noise associated with the result.

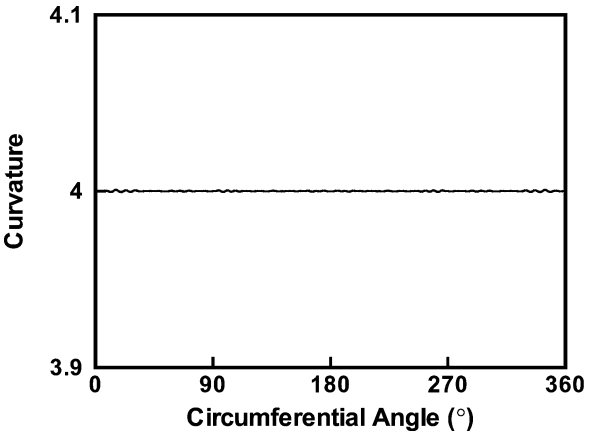

Fig. 6. The computed curvature along the circumference of the drop interface, from 0 to 360 degrees.

Fig. 6. Courbure calculée le long de la circonférence de l'interface de la goutte, de 0 à 360 degrés.

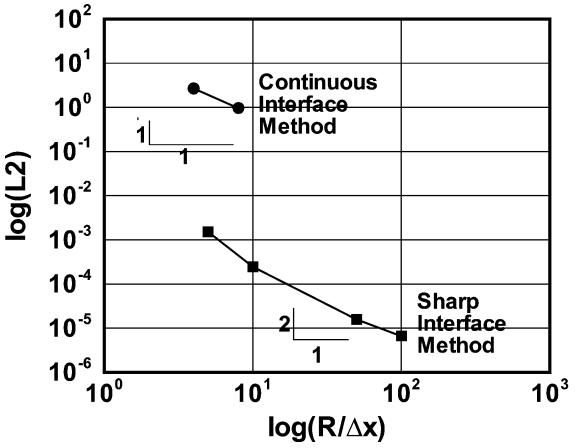

Fig. 7. Comparison between the sharp and continuous interface methods based on the error norms defined in Eq. (6).

Fig. 7. Comparaison entre les méthodes avec une interface discontinue et une interface de transition continue basées sur les normes d'erreur définies dans l'Éq. (6).

Table 1
Effect of the grid size for a spherical drop in static equilibrium

$R/\Delta x$	ρ_l/ρ_v	$\Delta p_{\text{num}}/\Delta p_{\text{exact}}$	Pressure error norm L_{2B}
5	1000.0	0.9988	1.509E-03
10	1000.0	0.9998	2.452E-04
50	1000.0	1.000	1.612E-05
100	1000.0	1.000	6.632E-06

Next, we assess the order of accuracy of the SIM solution. The assessment is based on the overall pressure difference, defined as:

$$\Delta p_{\text{num}} = \frac{1}{N_{\text{in}}}\sum_{n=1}^{N_{\text{in}}} P_n - \frac{1}{N_{\text{out}}}\sum_{n=1}^{N_{\text{out}}} P_n \tag{5}$$

where, N_{in} is the number of cells inside the bubble and N_{out} is the cells outside; p_n is the pressure in each cell. In Fig. 7 and Table 1, the solutions of SIM and CIM (using the immersed boundary method) are compared with varying grid size, Δx. The relative error between the theoretical and numerical pressure difference can be expressed in terms of L_2-norm. L_2-norm of the error was defined as:

$$L_{2B} = \sqrt{\frac{1}{N_{\text{in}}}\sum_{n=1}^{N_{\text{in}}} \frac{(P_{\text{num}} - P_{\text{exact}})^2}{P_{\text{exact}}^2}} \tag{6}$$

Fig. 7 and Table 1 confirm that SIM offers noticeably lower error with approximately overall second-order accuracy. For comparison purpose, representative results based on the CIM [19] are also depicted in Fig. 7; it yields first-order accuracy and the errors are several orders of magnitude larger for all grid resolutions. For more information, we refer to Ye et al. [20]. The results reported here are representative; the essence of the findings does not change with respect to the pressure and surface tension values.

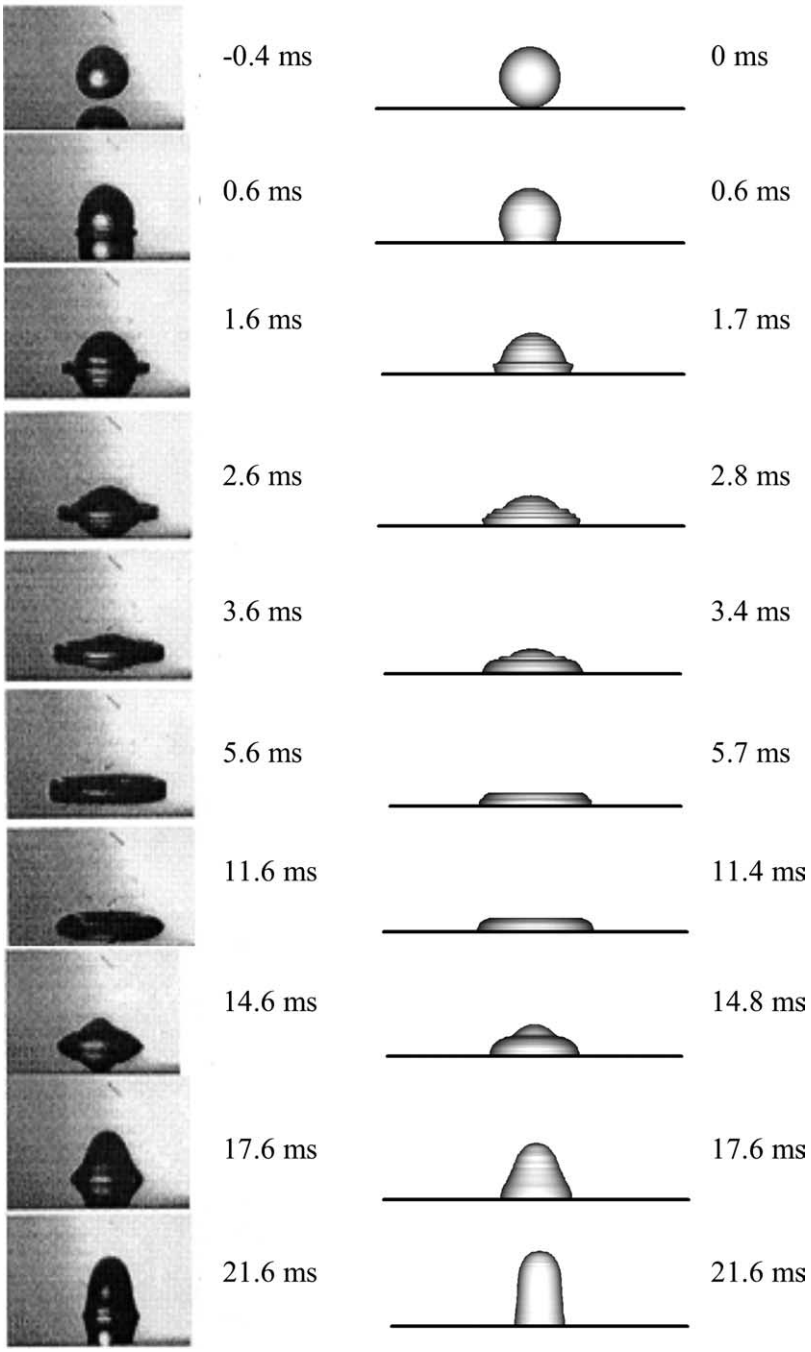

Fig. 8. Water droplet impinging on polycarbonate surface $Re = 3200$, $We = 30$, $Fr = 17$. Left column images of Kim and Chun [21] experimental results. Right column presents numerical simulation.

Fig. 8. Gouttelette d'eau faisant un impact sur une surface en polycarbonate $Re = 3200$, $We = 30$, $Fr = 17$. À gauche, une colonne d'images des résultats expérimentaux de Kim et Chun [21]. À droite, une colonne montrant les simulations numériques.

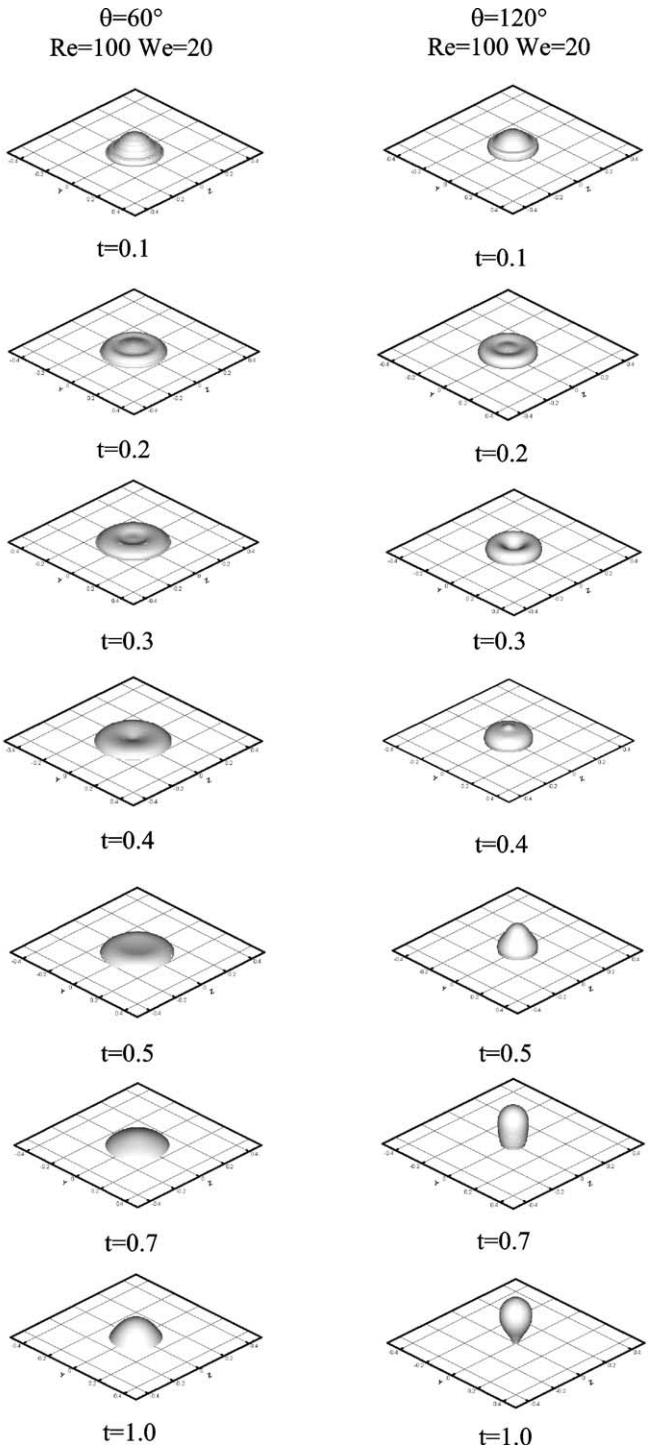

Fig. 9. Droplet shapes at different time instants for varied static contact angles.

Fig. 9. Formes des gouttes à différents instants pour divers angles de contact statique.

3.2. Impact of a liquid drop on a polycarbonate surface

The computations of a water droplet impinging on a polycarbonate surface are now compared with the experiments of Kim and Chun [21]. Initially, a spherical droplet of diameter d is placed on the surface and given an impact velocity U. The bottom wall of the computational domain, where the drop impacts, is kept at a constant temperature $T_w = 1.0$, and the top and side walls are adiabatic. Initially, both the liquid and gas phases are at $T_0 = 0$. The contact angle in the simulation is held unchanged. For more information, we refer to Francois and Shyy [10,22]. A direct comparison between 3D view generated from numerical simulation and the photographs of the droplet shapes is shown in Fig. 8 at the corresponding time instants, for water and ink, respectively. In both cases the results are in reasonably good agreement with the experiment. For the density, viscosity and surface tension values of water and ink, we have employed the same values that are reported in [21]. We have considered the gas phase 1000 time less dense and 20 times less viscous than the liquid phase. The non-dimensional numbers for the water drop are $Re = 3200$, $We = 30$ and $Fr = 17$, where the Reynolds (Re), Weber (We) and Froude (Fr) numbers are:

$$Re = \frac{\rho_l U d}{\mu_l} \tag{7}$$

$$We = \frac{\rho_l U^2 d}{\sigma} \tag{8}$$

$$Fr = \frac{U^2}{g d} \tag{9}$$

3.3. Effect of contact angle on deformation

Three contact angle values are considered: $60°, 80°, 100°$, and $120°$ to help assess the influence of the contact dynamics. These computations are all done for $Re = 100$ and $We = 20$. The instantaneous droplet shapes are presented in Fig. 9 for two contact angles, $60°$ and $120°$. One notices that for larger contact angle values, both maximum and equilibrium values of the spreading coefficient decrease and the amplitude of the recoiling oscillations becomes greater, eventually reaching a point beyond which the droplet bounces back, as happens for $\theta = 120°$. Of course, in reality, the contact angle varies as function of the speed and direction of the contact line [7]. This and related aspects have been studied. For more information, we refer to Francois and Shyy [10,22].

4. Conclusions

The SIM is fundamentally consistent with continuum theory, while the SIM offers more numerical convenience because one does not have to distinguish different zones or materials individually. The SIM is more demanding computationally because the field equations in each phase need to be coupled between different materials/phases, and explicitly linked with the interfacial conditions. In return, second-order accuracy is achieved as compared to the first-order accuracy in CIM, indicating that the SIM can handle more complicated problems requiring higher accuracy. Our view is that for many multi-fluid problems, such as the drop and bubble dynamics, the CIM can work quite well in practice [8,10,22]. This is especially true in view of the substantial uncertainties in transport properties. On the other hand, if details of the interfacial characteristics are critical and demanding in estimation, then the SIM will be a suitable approach. A good example is the solidification dynamics at the morphological scale [4,14,15]. Many outstanding problems, especially those in three spatial dimensions, involving topological changes such as break-up and merger, and requiring accurate geometric estimations remain challenging. There is ample room for further development in this scientifically interesting and practically important area.

Acknowledgements

The present work is supported by the NASA University Research, Engineering and Technology Institute (URETI) program. The results presented are based on the collaboration with Drs. M. Francois, H.S. Udaykumar, and T. Ye, indicated by the references cited. The author thanks Dr. Mohammad El Ganaoui for his kind invitation to write the present article.

References

[1] G. Ryskin, L.G. Leal, Numerical solution of free boundary problems in fluid mechanics, Parts I, II, III, J. Fluid Mech. 148 (1984) 1–43.
[2] F.H. Harlow, J.E. Welch, Numerical calculation of time-dependent viscous incompressible flow of fluid with free surface, Phys. Fluids 8 (1965) 2182–2189.
[3] W. Shyy, S.-J. Liang, D.Y. Wei, Effect of dynamic perturbation and contact condition on edge-defined fibre growth characteristics, Int. J. Heat Mass Transfer 37 (1994) 977–987.
[4] W. Shyy, H.S. Udaykumar, M.M. Rao, R.W. Smith, Computational Fluid Dynamics with Moving Boundaries, Hemisphere, Washington, DC, 1996.
[5] C.S. Peskin, Numerical analysis of blood flow in the heart, J. Comput. Phys. 25 (1977) 220–252.
[6] D. Gueyffier, J. Li, A. Nadim, R. Scardovelli, S. Zaleski, Volume-of-fluid interface tracking with smoothed surface stress methods for three-dimensional flows, J. Comput. Phys. 152 (1999) 423–456.
[7] W. Shyy, Computational Modeling for Fluid Flow and Interfacial Transport, Elsevier, Amsterdam, Netherlands, 1994.
[8] W. Shyy, M. Francois, H.S. Udaykumar, N. N'dri, R. Tran-Son-Tay, Moving boundaries in micro-scale biofluid dynamics, Appl. Mech. Rev. 54 (2001) 405–453.
[9] S. Osher, J.A. Sethian, Fronts propagating with curvature dependent speed: alogorithms based on Hamilton–Jacobi formulations, J. Comput. Phys. 79 (1988) 12–49.
[10] M. Francois, W. Shyy, Micro-scale drop dynamics for heat transfer enhancement, Prog. Aerospace Sci. 38 (2002) 275–304.
[11] M.W. Williams, D.B. Kothe, E.G. Puckett, Accuracy and convergence of continuum surface-tension models, in: W. Shyy, R. Narayanan (Eds.), Fluid Dynamics at Interfaces, Cambridge University Press, 1999.
[12] D. Lörstad, M. Francois, W. Shyy, L. Fuchs, Volume of fluid and immersed boundary investigations of a single rising droplet, in: 41st Aerospace Sciences Meeting & Exhibit, 2003, Paper No. 2003-1282.
[13] R.J. LeVeque, Z. Li, The immersed interface method for elliptic equations with discontinuous coefficients and singular sources, SIAM J. Numer. Anal. 31 (1994) 1019.
[14] H.S. Udaykumar, W. Shyy, M.M. Rao, ELAFINT: a mixed, Eulerian–Lagrangian method for fluid flows with complex and moving boundaries, Int. J. Numer. Methods Fluids 22 (1996) 691–712.
[15] H.S. Udaykumar, R. Mittal, W. Shyy, Computation of solid–liquid phase fronts in the sharp interface limit on fixed grids, J. Comput. Phys. 153 (1999) 535–574.
[16] T. Ye, W. Shyy, J.N. Chung, A fixed-grid, sharp-interface method for bubble dynamics and phase change, J. Comput. Phys. 174 (2001) 781–815.
[17] T. Ye, R. Mittal, H.S. Udaykumar, W. Shyy, An accurate Cartesian grid method for viscous incompressible flows with complex immersed boundaries, J. Comput. Phys. 156 (1999) 209–240.
[18] G. Farin, Curves and Surface for Computer-Aided Geometric Design, A Practical Guide, fourth ed., Academic Press, 1997.
[19] D.B. Kothe, W.J. Rider, S.J. Mosso, J.S. Brock, J.I. Hochstein, Volume tracking of interfaces having surface tension in two and three dimensions, AIAA paper 96-0859, 1996.
[20] T. Ye, W. Shyy, C.-F. Tai, J.N. Chung, Assessment of a sharp interface method for drop in equilibrium, Comput. & Fluids, in press.
[21] H.-Y. Kim, J.-H. Chun, The recoiling of liquid droplets upon collision with solid surfaces, Phys. Fluids 13 (2001) 643–659.
[22] M. Francois, W. Shyy, Computations of drop dynamics with the immersed boundary method; Part 1 – Numerical algorithm and buoyancy induced effect, Numer. Heat Transfer Part B 44 (2003) 101–118;
M. Francois, W. Shyy, Computations of drop dynamics with the immersed boundary method; Part 2 – Drop impact and heat transfer, Numer. Heat Transfer Part B 44 (2003) 119–143.
[23] M. Francois, E. Uzgoren, J. Jackson, W. Shyy, Multigrid computations with the immersed boundary technique for multiphase flows, Int. J. Numer. Methods Heat and Fluid Flow 14 (2004) 98–115.